ELSEVIER

Journal of Organometallic Chemistry 531 (1997) 227–235

Journal of Organometallic Chemistry

Carbonylation reaction of alkyl complexes of iron and molecular structure of *cis,trans*-[Fe(CO)$_2$(PMe$_3$)$_2$(CH$_3$)I] and *trans,trans*-[Fe(CO)$_2$(PMe$_3$)$_2$(CH$_3$)I]

Gianfranco Bellachioma [a], Giuseppe Cardaci [a,*], Alceo Macchioni [a], Gustavo Reichenbach [a], Elisabetta Foresti [b], Piera Sabatino [b,*]

[a] *Dipartimento di Chimica, Università di Perugia, Via Elce di Sotto, 8, I-06100 Perugia, Italy*
[b] *Dipartimento di Chimica "G. Ciamician", Università di Bologna, Via Selmi 2, I-40126 Bologna, Italy*

Received 5 August 1996; revised 14 October 1996

Abstract

The carbonylation reaction of *cis,trans*-[Fe(CO)$_2$(PMe$_3$)$_2$(CH$_3$)I] (**Me**) to *cis,trans*-[Fe(CO)$_2$(PMe$_3$)$_2$(COCH$_3$)I] (**Ac**) and the isomerization of **Ac** to *trans,trans*-[Fe(CO)$_2$(PMe$_3$)$_2$(COCH$_3$)I] (**At**) were studied in polar and apolar solvents. The results suggest that the first step of the carbonylation is the formation of the ionic intermediate [Fe(CO)$_3$(PMe$_3$)$_2$(CH$_3$)]I (**In**); complexes **Ac** and **At** are both formed from the intermediate **In** at different rates due to the differential cooperative effect of the anion. Further information was obtained by a structural study of complexes **Me** and *trans,trans*-[Fe(CO)$_2$(PMe$_3$)$_2$(CH$_3$)I] (**Mt**), using single crystal X-ray diffraction. The structure models were refined to $R = 0.034$ for 2270 independent reflections for **Me** and $R = 0.056$ for 2381 independent reflections for **Mt**. Crystal data: monoclinic, space group $P2_1/c$ for both molecules: $a = 13.656(2)$, $b = 9.032(3)$, $c = 13.880(6)$ Å, $\beta = 106.78(3)°$ for **Me**; $a = 13.818(3)$, $b = 8.957(2)$, $c = 13.826(3)$ Å, $\beta = 105.21(3)°$ for **Mt**. Both complexes present octahedral coordination of the ligands around the metal centre.

Keywords: CO insertion; Iron complexes; X-ray diffraction; Mechanism; Equilibrium constants

1. Introduction

The insertion of carbon monoxide in the Fe–R bond of [Fe(CO)$_2$(PMe$_3$)$_2$RX] (X = Cl, Br, I) has been extensively studied [1–6]. The reaction proceeds in two steps according to Scheme 1 (the same scheme is valid for the complexes having Cl or Br instead of I).

The structure of the methyl and acetyl complexes has been previously described [7]. The stereochemistry of the reaction has been clarified by ^{13}CO labelling experiments using ^{13}C and ^{31}P NMR spectroscopy to characterize stereoisomers that form [1,6].

In contrast, only a kinetic study has been carried out for X = CN [2] and the results are in agreement with a migratory insertion mechanism [8,9].

For X = Cl, Br, and I, the reaction rate is too fast to be followed also in a moderately polar solvent like CH_2Cl_2; however, important observations have been reported:

(a) a strong solvent effect on the rate [1,6];

(b) the formation of $^{13}COCH_3$ during the labelling experiments [1,10,11];

(c) the dependence of the isomerization on the CO pressure [6,10,11].

Point (b) suggests that the mechanism proceeds by ionization of the Fe–X bond with the formation of the ionic complex [Fe(CO)$_3$(PMe$_3$)$_2$CH$_3$]$^+$X$^-$ (**In**). Two ionization mechanisms have been hypothesized: the first occurs by ionization of the previously-formed acetyl complex [1]; the second by X substitution with CO in the methyl complex (**Me**) [6]. The formation of the ionic intermediate explains the strong solvent effect and supports the change of mechanism suggested by Wright and Baird [6] on passing from less polar to more polar solvents.

On the other hand, the labelling of $^{13}COCH_3$ is also observed in apolar solvents (*n*-hexane, toluene), but at a

* Corresponding authors.

0022-328X/97/$17.00 © 1997 Elsevier Science S.A. All rights reserved.
PII S0022-328X(96)06878-7

slower rate. This can be explained on the basis of an ionization process which occurs by intimate ion pair formation as observed for the isotopomerization process of monolabelled ^{13}CO complexes [12].

In this work, we report the results of a study of the carbonylation reaction in polar and apolar solvents and the X-ray molecular structure of complexes **Mc** and **Mt** carried out in order to obtain further information on the reaction mechanism.

2. Experimental details

2.1. General

cis,trans-$[Fe(CO)_2(PMe_3)_2(CH_3)I]$ (**Mc**), *cis,trans*-$[Fe(CO)_2(PMe_3)_2(COCH_3)I]$ (**Ac**) and *trans,trans*-$[Fe(CO)_2(PMe_3)_2(COCH_3)I]$ (**At**) were prepared as described in Refs. [9,12]; *trans,trans*-$[Fe(CO)_2(PMe_3)_2(CH_3)I]$ (**Mt**) was prepared as described in Ref. [4]. Toluene was purified by a standard method [13]. Other solvents were commercial spectral grade and used without purification. IR spectra were recorded on a Perkin–Elmer 983 spectrophotometer or on an 1725X FT-IR Perkin–Elmer spectrophotometer.

2.2. Reaction of Mc with CO in various solvents

The reaction was carried out in CH_2Cl_2, *n*-propanol, *n*-pentanol, and nitromethane at 25 °C and at P_{CO} = 1 atm and followed by using IR spectroscopy. In all the solvents, the first product was the ionic complex **In** (ν_{CO} = 2084(vw), 2021(vs) cm^{-1} in CH_2Cl_2), then complex **At** was formed. The rate of **At** formation decreased on passing from CH_2Cl_2 to nitromethane. In nitromethane the formation of the salt was instantaneous, the formation of **At** was slow and continued until the equilibrium concentration was reached. In CH_2Cl_2, the initial formation of the salt was quickly followed by the formation of **At** and, at the end of the reaction, the salt disappeared. It was not possible to follow the formation of **Ac** due to the overlap of its CO stretching bands (ν_{CO} = 2012(s), 1959(s) cm^{-1} in CH_2Cl_2) with the CO stretching bands of **In** and **At** (ν_{CO} = 2044(vw), 1961(vs) cm^{-1} in CH_2Cl_2).

2.3. Reaction of trans-$[Fe(CO)_3(PMe_3)_2CH_3]BPh_4$ and NBu_4I

Complex $[Fe(CO)_3(PMe_3)_2CH_3]BPh_4$ [7] (100 mg) was dissolved in CH_2Cl_2 (15 ml) and thermostatted at 0 °C. NBu_4I (75 mg) was then added. **Ac** and **Mc** formed (ratio 2/1) instantaneously (1 min). The concentration of **Mc** was lower than the equilibrium value but it increased until it reached the equilibrium value; then the reaction slowly gave **At**. The experiment was repeated at 15 °C and the course of the reaction was similar.

2.4. Kinetic measurements

The kinetic measurements of the carbonylation reaction were carried out in toluene. The carbon monoxide concentration at different temperatures was interpolated on the basis of literature data [14,15]. Different CO pressures (0.025–1 atm) were obtained by dilution with nitrogen in a Mohr bottle. For reactions carried out at temperatures higher than 48 °C, the partial pressure was corrected for the vapour pressure of toluene [16]. All measurements were carried out in the dark, due to the light sensitivity of the **Mc** and **Mt** complexes.

2.4.1. Carbonylation reactions

The reaction was studied in the temperature range 10–30 °C. In a typical run, a solution of **Mc** complex [ca. $(8–15) \times 10^{-3}$ M] was introduced in a thermostatted reactor filled with the gas mixture and stirred with a magnetic bar. After an initial period, depending on the temperature, a constant ratio of **[Ac]/[Mc]** was reached; the rate of conversion to the complex **At** was then followed, by measuring the IR spectrum in the range 2100–1800 cm^{-1} at various times. The disappearance of complex **Mc** was followed by the absorbances of the two CO stretching bands at 1998 and 1940 cm^{-1}; the disappearance of **Ac** was followed by the absorbances of the CO stretching band at 2018 cm^{-1}. The formation of complex **At** could not be followed due to the overlap of its CO stretching band at 1960 cm^{-1} with the CO stretching band of complex **Ac** at 1963 cm^{-1}.

In the CO pressure range used, the carbonylation to

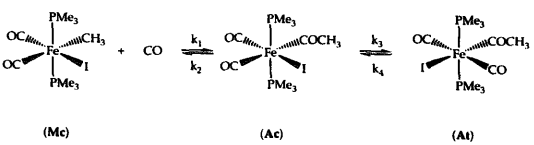

(**Mc**) (**Ac**) (**At**)

Scheme 1.

complex **At** was complete and the pseudo first-order rate constants k_{obs} were measured using Eq. (1).

$$\ln\frac{D_o}{D_t} = k_{obs}t \quad (1)$$

in which D_o is the absorbance of the solution when a constant [Ac]/[Mc] ratio is reached and D_t is the absorbance at the various t. For each kinetic run, the error in k_{obs} is less than 2%. The data are presented as the mean value of four measurements at the same concentration of complex.

2.4.2. Decarbonylation reactions

Complex **At** was decarbonylated to complex **Mc** in the temperature range 48–60 °C. With a CO pressure range of 0.025–0.1 atm the reaction went to equilibrium. In each kinetic run, the CO concentration was held constant in order to operate under pseudo first-order conditions. The toluene solution of **At** [ca. $(8–16)\times 10^{-3}$ M] was saturated with the gas mixture and introduced into a thermostatted reactor. The kinetic runs were monitored by withdrawing solution aliquots at various times and recording IR spectra in the 2100–1800 cm^{-1} range. The concentration of **At** was obtained from the absorbance of the CO stretching band at 1960 cm^{-1} and the concentration of **Mc** from that of the two CO stretching bands at 1998 and 1940 cm^{-1}. The concentration of **Ac** was negligible under the experimental conditions used.

The pseudo first-order rate constants k_{fwd} were determined by following the disappearance of the **At** complex as well as the appearance of the **Mc** complex using Eq. (2), where D_o, D_e and D_t are the absorbances of **Mc** and **At** at zero time, equilibrium, and t time respectively.

$$\ln\frac{(D_o - D_e)}{(D_t - D_e)} = (k_{fwd} + k_{rev})t = k_{fwd}\frac{a}{x_e}t \quad (2)$$

k_{fwd} and k_{rev} are the pseudo first-order rate constants for the forward and the reverse reactions respectively; a is the starting concentration of complex **At** and x_e is the equilibrium concentration of complex **Mc**. The agreement between the disappearance of **At** and the appearance of **Mc** is better than 3%. The reported data are the mean values of four measurements and the average deviation is less than 5%.

2.5. X-ray crystallography

Diffraction intensities were collected at room temperature by the ω–2θ scan method on a graphite monochromatized Enraf–Nonius CAD-4 diffractometer and reduced to F_o^2 values. Both structures were solved by direct methods and refined by full matrix least squares calculations. For all computations the SHELXS86 [17] and SHELX93 [18] packages of crystallographic programs were used. Thermal vibrations were treated anisotropically for all non-H atoms. In compound **Mt**, the methyl groups bound to P(2) were found to be affected by high thermal motions and some restraints had to be applied to the P–C bond lengths. In both compounds, the Fe-bound methyl hydrogen atoms were experimentally located in difference Fourier maps. All the remaining H atoms were positioned geometrically (C–H 0.96 Å) and refined with adequate constraints, tying their temperature factors to be 1.5 times those of their parent atoms. Final difference Fourier maps showed

Table 1
Pseudo first-order rate constants [a] k_{obs} in toluene for the carbonylation reaction

T (°C)	P_{CO} (atm)	$10^3\times$[CO] (M)	$10^4\times k_{obs}$ (s^{-1})
10.7	1.00	7.90	1.98 (0.02)
	0.50	3.95	1.90 (0.01)
	0.30	2.36	1.84 (0.02)
	0.15	1.19	1.63 (0.02)
	0.10	0.79	1.48 (0.01)
	0.08	0.59	1.34 (0.01)
20.0	1.00	7.21	6.93 (0.05)
	0.50	3.61	6.58 (0.04)
	0.25	1.78	5.71 (0.04)
	0.15	1.17	4.90 (0.06)
	0.10	0.72	4.07 (0.07)
25.0	1.00	6.77	13.7 (0.1)
	0.50	3.39	12.6 (0.1)
	0.25	1.70	10.4 (0.2)
	0.10	0.67	7.06 (0.10)
30.0	1.00	6.41	25.6 (0.3)
	0.50	3.16	21.8 (0.2)
	0.25	1.59	17.0 (0.2)
	0.18	1.12	16.0 (0.3)
	0.10	0.64	11.4 (0.3)

[a] The values in parentheses are the mean deviations of four measurements.

Table 2
First-order rate constants k_{fwd} and equilibrium constants K_e for the decarbonylation reaction in toluene at various temperatures

T (°C)	P_{CO} (atm)	$10^4\times$[CO] (M)	$10^3\times k_{fwd}$ [a] (s^{-1})	$10^4\times K_e$ [a] (M)
59.8	0.100	4.20	2.77 (0.10)	2.70 (0.10)
	0.050	2.08	2.54 (0.08)	2.80 (0.08)
	0.025	1.05	2.66 (0.12)	2.75 (0.08)
55.7	0.100	4.48	1.61 (0.08)	2.17 (0.05)
	0.050	2.24	1.74 (0.06)	2.20 (0.10)
	0.025	1.12	1.68 (0.10)	2.16 (0.10)
52.0	0.050	2.36	1.27 (0.05)	1.86 (0.08)
	0.025	1.18	1.35 (0.07)	1.85 (0.05)
48.0	0.025	1.25	0.79 (0.02)	1.45 (0.06)

[a] The values in parentheses are the mean deviations of four measurements.

Table 3
Crystal data and details of measurements for **Me** and **Mt**

	Me	**Mt**
Formula	$C_9H_{21}FeIO_2P_2$	$C_9H_{21}FeIO_2P_2$
Mol wt	405.9	405.9
Temperature (K)	293	293
System	monoclinic	monoclinic
Space group	$P2_1/c$	$P2_1/c$
a (Å)	13.656(2)	13.818(3)
b (Å)	9.032(3)	8.957(2)
c (Å)	13.880(6)	13.826(3)
β (deg)	106.78(3)	105.21(3)
V (Å^3)	1639(1)	1651(1)
Z	4	4
$F(000)$	800	800
λ(Mo Kα) (Å)	0.71069	0.71069
μ(Mo Kα) (cm^{-1})	29.8	29.6
θ-range (deg)	2.5–25	2.5–25
ω-scan width (deg)	0.9	0.7
Octants explored (h_{min},h_{max}; k_{min},k_{max}; l_{min},l_{max})	−16,16; 0,10; 0,16	−16,16; 0,10; 0,16
Measured reflections	3010	3041
Unique observed reflections	2879	2908
Unique observed reflections [$I_o > 2\sigma(I_o)$]	2270	2381
No. of refined parameters	136	137
GOF on F^2	1.02	1.13
Final R indices [$I > \sigma(I)$] R_1 (on F), wR_2 (on F^2)	0.034, 0.082	0.056, 0.157
Final R indices (all data) R_1 (on F), wR_2 (on F^2)	0.048, 0.109	0.067, 0.177

residual peaks lower than 0.8 e Å^{-3} in the proximity of the iodine atom for both compounds

3. Results

The pseudo first-order rate constants k_{obs} for the carbonylation reaction at various temperatures are given in Table 1. k_{obs} increases with increased CO concentration and tends asymptotically to a constant value.

The pseudo first-order rate constants for the decarbonylation reaction k_{fwd} at various temperatures are given in Table 2, which also includes the equilibrium constants for the decarbonylation reaction K_c. In the range of CO concentration used (0.025–0.1 atm), k_{fwd}

Table 4
Atomic coordinates (10^4) and equivalent isotropic displacement parameters (Å$^2 \times 10^3$) for **Me**

	x	y	z	U_{eq} [a]
Fe	2585(1)	321(1)	8649(1)	49(1)
I	1603(1)	2456(1)	9362(1)	64(1)
P(1)	3437(1)	2128(2)	8110(1)	62(1)
P(2)	1541(1)	−1343(2)	9060(1)	62(1)
O(1)	3551(3)	−1956(6)	7806(4)	112(2)
O(2)	4093(3)	254(5)	10627(3)	97(1)
C(1)	3179(4)	−1053(7)	8147(4)	70(1)
C(2)	3490(4)	279(6)	9853(3)	62(1)
C(3)	1526(4)	361(6)	7218(4)	68(1)
C(4)	2696(4)	3610(6)	7365(4)	75(1)
C(5)	4375(5)	3140(8)	9081(5)	102(2)
C(6)	4174(4)	1499(9)	7286(5)	94(2)
C(7)	172(4)	−994(7)	8629(5)	86(2)
C(8)	1759(6)	−1660(9)	10387(5)	103(2)
C(9)	1585(6)	−3193(7)	8565(7)	116(3)

[a] U_{eq} is defined as one-third of the trace of the orthogonalized U_{ij} tensor.

Table 5
Atomic coordinates (10^4) and equivalent isotropic displacement parameters (Å$^2 \times 10^3$) for **Mt**

	x	y	z	U_{eq} [a]
I	8466(1)	2403(1)	5712(1)	76(1)
Fe	7482(1)	287(1)	6444(1)	57(1)
P(1)	6591(1)	2127(3)	6918(2)	72(1)
P(2)	8470(2)	−1429(3)	5992(2)	84(1)
O(1)	5998(5)	−24(10)	4526(5)	116(2)
O(2)	8827(6)	185(9)	8472(5)	112(2)
C(1)	6588(6)	113(9)	5286(6)	74(2)
C(2)	8305(6)	261(9)	7665(6)	74(2)
C(3)	6656(7)	−1365(11)	6928(8)	101(3)
C(4)	5720(8)	1594(14)	7644(9)	118(4)
C(5)	7308(7)	3575(10)	7706(7)	90(2)
C(6)	5776(8)	3192(14)	5901(8)	111(3)
C(7)	9818(4)	−1004(13)	6443(8)	137(5)
C(8)	8329(9)	−1618(16)	4651(4)	157(6)
C(9)	8431(10)	−3341(8)	6416(11)	232(12)

[a] U_{eq} is defined as one-third of the trace of the orthogonalized U_{ij} tensor.

did not exhibit any appreciable variation. It was not experimentally possible to extend the CO concentration range.

Crystal data and details of measurements for **Mc** and **Mt** are reported in Table 3. Atomic coordinates and equivalent isotropic displacement parameters are given in Tables 4 and 5.

4. Discussion

4.1. Description of the molecular structure of complex Mc and Mt

The molecular structures of **Mc** and **Mt** are shown in Figs. 1 and 2 respectively. Relevant bond parameters are reported in Table 6. The structural study fully confirms the stereogeometry of the two isomers. **Mc** has idealized C_s symmetry with two axial phosphine ligands and cis-coordination of the equatorial CO groups. **Mt** has C_{2v} idealized symmetry with trans-coordination of the phosphine and CO ligands.

The Fe–P bond lengths are almost equal within the experimental errors in both complexes [2.253(2) and 2.255(2) Å in **Mc**; 2.255(2) and 2.250(2) Å in **Mt**]. The correspondence of values is higher than expected, but this is not surprising in view of the fact that the crystals of the two species are isomorphous, i.e. the packing forces are almost identical within either crystal. This latter circumstance is very favourable and allows one to discuss as significant all the differences in bond distances in terms of intramolecular factors.

There are three different kinds of Fe–CO interaction in the two isomers: (i) CO trans to CO [average Fe–C 1.76, C–O 1.15 Å]; (ii) CO trans to methyl [Fe–C 1.769(4), C–O 1.149(5) Å] and iii) CO trans to iodide [Fe–C 1.735(6), C–O 1.134(6) Å]. These figures indi-

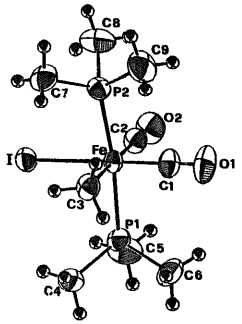

Fig. 1. Molecular structure of complex **Mc**.

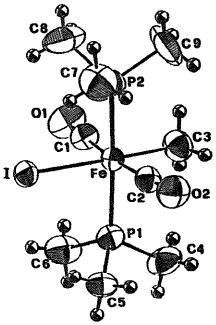

Fig. 2. Molecular structure of complex **Mt**.

Table 6
Selected bond lengths (Å) and angles (deg) for **Mc** and **Mt**

	Mc	Mt
Fe–C(1)	1.735(6)	1.753(8)
Fe–C(2)	1.769(4)	1.772(8)
Fe–C(3)	2.092(5)	2.083(7)
Fe–P(1)	2.253(2)	2.255(2)
Fe–P(2)	2.255(2)	2.250(2)
Fe–I	2.695(1)	2.681(1)
P(1)–C(4)	1.811(5)	1.821(9)
P(1)–C(5)	1.816(6)	1.813(8)
P(1)–C(6)	1.819(6)	1.823(9)
P(2)–C(7)	1.819(5)	1.842(4)
P(2)–C(8)	1.802(6)	1.821(4)
P(2)–C(9)	1.815(7)	1.815(5)
O(1)–C(1)	1.134(6)	1.154(9)
O(2)–C(2)	1.149(5)	1.161(10)
C(1)–Fe–C(2)	94.8(2)	172.5(4)
C(1)–Fe–C(3)	84.7(2)	85.2(4)
C(2)–Fe–C(3)	179.4(2)	87.3(4)
C(1)–Fe–P(1)	92.2(2)	91.3(3)
C(2)–Fe–P(1)	92.4(2)	89.8(3)
C(3)–Fe–P(1)	87.4(2)	92.2(3)
C(1)–Fe–P(2)	91.6(2)	91.1(3)
C(2)–Fe–P(2)	93.8(2)	88.3(3)
C(3)–Fe–P(2)	86.4(2)	91.6(3)
P(1)–Fe–P(2)	172.4(1)	175.6(1)
C(1)–Fe–I	177.8(2)	91.4(3)
C(2)–Fe–I	87.4(2)	96.1(3)
C(3)–Fe–I	93.2(2)	176.6(3)
P(1)–Fe–I	87.88(4)	87.9(1)
P(2)–Fe–I	88.05(4)	88.5(1)
C(4)–P(1)–Fe	117.9(2)	117.3(4)
C(5)–P(1)–Fe	116.1(2)	116.3(3)
C(6)–P(1)–Fe	114.5(3)	115.6(3)
C(7)–P(2)–Fe	117.8(2)	113.5(4)
C(8)–P(2)–Fe	115.8(2)	115.8(4)
C(9)–P(2)–Fe	115.2(3)	118.9(5)
O(1)–C(1)–Fe	178.7(5)	179.0(8)
O(2)–C(2)–Fe	178.6(5)	177.1(8)

cate that the trans-influence of the Me group on the CO ligand is substantially equivalent to that of the CO itself and that the iodide ligand is the least effective in destabilizing the Fe–CO interaction.

A similar trend has been observed in the closely related osmium complex *cis,trans*-$Os(CO)_2(PMe_3)_2(Me)I$ [19], in which the Os–CO interactions are 1.81(1) and 1.89(1) Å when the trans ligands are I and Me respectively.

There are two kinds of Fe–I interaction: (i) I trans to Me [2.681(1) Å] in **Mt** and (ii) I trans to CO [2.695(1) Å] in **Mc**. Both fall in the upper range of usually found values [cf. 2.678(2) in $[Fe(CO)(PMePh_2)(\eta^2\text{-}COCH_3)I] \cdot 2CH_2Cl_2$ [20] and 2.623 Å given as standard value] [21].

Having demonstrated that the trans influencing abilities of Me and CO are substantially equivalent, the slightly longer Fe–I distance in **Mc** can be attributed to the non-bonded interaction with the methyl hydrogen in the equatorial plane [I ··· H(3A) 3.122(5) Å, C(Me)–Fe–I 93.2(2)°, C(CO)–Fe–I 87.4(2)°].

Finally, two kinds of Fe–C(Me) distance occur in the two complexes: (i) trans to the CO group in **Mc** [2.092(5) Å] and (ii) trans to the iodide in **Mt** [2.083(7) Å]. Both values fall well within the range of those found for the few octahedral d^6 iron complexes known up to date [22], and no significant difference between them is apparent.

A sterically and electronically comparable species, such as $Fe(CO)_2(CNBPh_3)(PMe_3)_2(CH_3)$ [23] exhibits bond distances strictly equivalent to those already discussed, i.e. Fe–P 2.256(1) and 2.245(1) Å, Fe–C(Me) 2.079(5) Å and Fe–CO 1.772(4) and 1.759(4) Å for the CO trans to methyl and triphenylborato-nitrilomethyl respectively. Sterically similar compounds such as $FeI(CO)_2(P(OPr^i)_3)_2$ [24], but differing in the phosphite bonding peculiarities with respect to the phosphine, show significant differences in bond lengths. The Fe–P phosphite distances [2.219(8) and 2.210(7) Å] are shorter because of the intrinsically smaller radius of the phosphorus bonded to three oxygens and its greater π-acidity. At the same time, on the equatorial plane, the distances involving σ-donor ligands are shrunk [Fe–I 2.618(6), Fe–C(alkyl) 2.05(2) Å], while the ones involving π-acceptor ligands are longer [Fe–CO 1.76(2) and 1.86(3) Å].

An asymmetric effect of the methyl hydrogens on the neighbouring ligands is also observed in **Mt** [C(2) ··· H(3A) 2.48 Å, C(3)–Fe–C(1) 85.2(4)°, C(3)–Fe–C(2) 87.3(4)°]. An asymmetric 'bending away' of the two carbonyl groups from the iodide is also observed in the same complex [I–Fe–C(1) 91.4(3)°, I–Fe–C(2) 96.1(3)°].

Finally, it should be mentioned that the phosphine ligands form a smaller P–Fe–P angle in **Mc** than in **Mt** [172.4(1)° and 175.6(1)° respectively], by bending towards the more distant iodide ligand.

In complex **Mt**, which exhibits the shorter Fe–I bond length, two symmetrical H(phosphine) ··· I interactions take place [C(5)–H(5) ··· I, 3.684 Å, C–H ··· I angle 124.4° and C(7)–H(7) ··· I, 3.582 Å, C–H ··· I angle 127.1°].

4.2. Kinetics and reaction mechanism

4.2.1. Polar solvents

The first product of the reaction between **Mc** and CO (P_{CO} = 1 atm) at room temperature is the ionic complex. Complex **At** is then formed from the ionic complex. It is difficult to follow the formation of complex **Ac** due to the overlap of the CO stretching bands with the ionic and **At** complexes. The rate of formation of **At** decreases as the dielectric constant of the solvent increases, in agreement with the trend observed in the reaction between ions of different sign [25]. The concentration of the ionic complex at equilibrium increases as the dielectric constant of the solvent increases. However, it is not analytically measurable in CH_2Cl_2.

Information on the rate of formation of **Ac** is obtained by the rate of the reaction of $[Fe(CO)_3(PMe_3)_2CH_3]BPh_4$ and NBu_4I in CH_2Cl_2. At 0 °C this reaction yields **Ac** and **Mc** instantaneously. The formation of **Ac** is faster than **Mc**. In fact successively the **[Mc]/[Ac]** ratio increases up to the equilibrium value.

On the basis of these observations, **Mc** immediately gives the ionic intermediate in polar solvents, which, in the second step, yields both **Ac** and **At**, but at different rates according to Scheme 2.

This mechanism is in agreement with that proposed by Wright and Baird [6], modified by the addition of the isomerization process by the ionic intermediate. The 'ionic isomerization' is a simple way to explain the high rate of formation of complex **Ac** relative to **At**. In fact, the I^- assists the methyl migration when it reacts in the cis position relative to the methyl ligand. This cooperative effect has already been observed in the decarbonylation process of analogous acetyl complexes of ruthenium [26] and in the isocyanide insertion of iron [27].

4.2.2. Apolar solvent

The carbonylation process in toluene follows Scheme 1. In the temperature range 10–30 °C $k_4 < k_3$ and the reaction goes to completion. The first step is so fast that it cannot be studied experimentally. In a previous paper [4], we reported some kinetic results for this step at 0 °C; unfortunately, those results referred to the diffusion of carbon monoxide from the gaseous phase to the solution. Due to this first step, an initial stage is observed in which complex **Ac** is formed until an equilib-

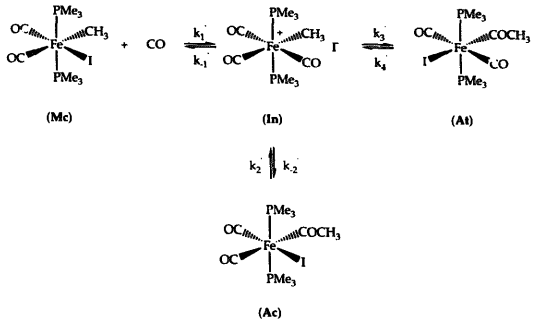

Scheme 2.

rium between **Ac** and **Mc** is attained. Subsequently, the [Ac]/[Mc] ratio remains constant up to 70% conversion.

The kinetics were followed under these conditions and treated according to the scheme of two consecutive reactions with the first step at equilibrium. On the basis of the mass conservation law and equilibrium requirements [28] the first-order rate constants k_{obs} follow Eq. (3)

$$k_{obs} = \frac{k_1 k_3 [CO]}{k_1 [CO] + k_2} \quad (3)$$

Rearrangement of Eq. (3) yields Eq. (4)

$$\frac{1}{k_{obs}} = \frac{1}{k_3} + \frac{k_2}{k_1 k_3 [CO]} \quad (4)$$

Plots of $1/k_{obs}$ vs. $1/[CO]$ give a straight line with $1/k_3$ as intercept and $k_2/(k_1 k_3)$ as the slope (Fig. 3). Values of k_3 and k_1/k_2 at various temperatures are given in Table 7. In the limits of experimental errors, k_1/k_2 values are in agreement with the experimental equilibrium constants for the first step of Scheme 1, measured previously [4].

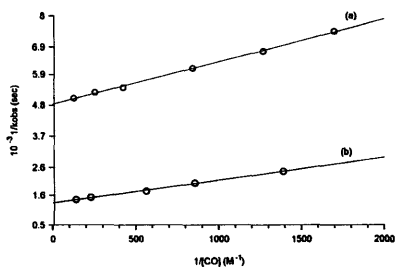

Fig. 3. $1/k_{obs}$ vs. $1/[CO]$ for the carbonylation reaction at 10.7 °C (a) and 20.0 °C (b).

The rate constant of the isomerization step k_3 is independent of CO concentration; therefore, the effect of CO pressure on the isomerization reaction, reported in the literature [5,6,10], is due to the carbonylation equilibrium of Scheme 1, which leads to the kinetic expression in Eq. (3); consequently, the isomerization reaction itself is not affected by CO pressure.

The decarbonylation reaction of **At** follows a first-order kinetic law (Table 2). Assuming the steady state approximation for complex **Ac**, the concentration of which is not experimentally measurable, $k_{fwd} = k_4 k_2/(k_3 + k_2)$. Since the first step attains equilibrium faster than the second step, $k_3 \ll k_2$ and then $k_{fwd} = k_4$.

Table 7
Summary of k_3, k_1/k_2, k_{fwd}, K_c, thermodynamic and activation parameters for the carbonylation and decarbonylation reactions

T (°C)	$10^4 \times k_3$ [a] (s^{-1})	k_1/k_2 [a] (M^{-1})	$10^3 \times k_{fwd}$ [b] (s^{-1})	$10^4 \times K_c$ [b] (M)
10.7	2.07 (0.03)	3155 (84)		
20.0	7.65 (0.36)	1576 (74)		
25.0	15.4 (0.70)	1268 (58)		
30.0	27.9 (4.5)	1048 (74)		
48.0			0.79 (0.10)	1.45 (0.06)
52.0			1.31 (0.05)	1.85 (0.01)
55.7			1.68 (0.07)	2.18 (0.02)
59.8			2.65 (0.15)	2.75 (0.05)

Thermodynamic and activation parameters [a]: $\Delta H^{\ddagger}(k_3) = 94(6)$ kJ mol^{-1}; $\Delta S^{\ddagger}(k_3)_{(298.1K)} = 17(21)$ J K^{-1} mol^{-1}, $\Delta H(k_1/k_2) = -41(22)$ kJ mol^{-1}; $\Delta S(k_1/k_2)_{(298.1K)} = -78(28)$ J K^{-1} mol^{-1}, $\Delta H^{\ddagger}(k_{fwd}) = 85(28)$ kJ mol^{-1}; $\Delta S^{\ddagger}(k_{fwd})_{(328.1K)} = -39(10)$ J K^{-1} mol^{-1}, $\Delta H(K_c) = 47(8)$ kJ mol^{-1}; $\Delta S(K_c)_{(328.1K)} = 73(3)$ J K^{-1} mol^{-1}.

[a] The values in parentheses are standard deviations at 95% confidence limits.

[b] The values in parentheses are mean deviations.

The thermodynamic and activation parameters, obtained by K_e and k_{fwd}, are in agreement with the previously measured thermodynamic parameters [4], though less precise due to the narrow range of temperatures that can be experimentally measured.

The results of both the carbonylation and decarbonylation kinetics do not provide direct information on the mechanism of the first step of Scheme 1. However, several indirect observations can be made.

(1) The variation of k_1k_3/k_2 with temperature allows the highest possible value of activation enthalpy and entropy of the first step to be calculated: $\Delta H_1^{\ddagger} = 53\ kJ\ mol^{-1}$ and $\Delta S_1^{\ddagger} = -61\ J\ K^{-1}\ mol^{-1}$. Neither value is in accord with a migratory insertion mechanism, which occurs with higher activation enthalpy [29]; they are, however, in agreement with an associative mechanism with CO to give the ionic intermediate of Scheme 2.

(2) In apolar solvents the formation of ionic compounds is unfavourable; however, the formation of intimate ion pairs has already been proposed for the isotopomerization of $[Fe(^{13}CO)(CO)(PMe_3)_2(CH_3)I]$ [12] and for halide exchange in **Mc** [30].

(3) The reaction rate between $[Fe(CO)_3(PMe_3)_2CH_3]^+$ and I^- increases with a decreased dielectric constant of the solvent. At 0 °C, the reaction in CH_2Cl_2 has a $t_{1/2} < 0.5$ min. It is therefore reasonable that in less polar solvents (toluene) the reaction rate is very high and can compensate the difficulty of forming a charge separation making the global ionization process an easy way for insertion.

On the basis of these observations, we suppose that the ionization mechanism of Scheme 2 is also active in apolar solvents.

Applications of the steady state approximation to the intermediate **In**, and rigorous equilibrium approximation to the species **Mc**, **Ac** and **At**, give

$$k_3 = \frac{k'_3k'_{-2}}{k'_2} \text{ and } \frac{k_1k_3}{k_2} = \frac{k'_3k'_1}{k'_{-1}} \text{ if } k'_3 \ll k'_2 + k'_{-1}$$

This last approximation is reasonable, since k'_3 is the rate determining step of the reaction. The $(k'_3k'_{-2})/k'_2$ and $(k'_3k'_1)/k'_{-1}$ values correspond to the rate constant for the formation of **At** starting from complex **Ac** and **Mc**, respectively.

Applying the same approximations to the decarbonylation reaction, yields $k_{fwd} = k'_{-1}k'_4/(k'_3 + k'_{-1})$, which, if $k'_{-1} \gg k'_3$, gives $k_{fwd} = k'_4$. So the formation of the ionic intermediate is the determining step of the decarbonylation reaction.

The carbonylation of **Mt** [4] is much slower than that of **Mc** ($t_{1/2} = 2 \times 10^3$ min vs. $t_{1/2} < 0.5$ min respectively). In spite of the different reactivity, the X-ray molecular structures of **Mt** and **Mc** do not show relevant differences in the Fe···CH_3 and Fe–I bonds. This indicates that there is no strong difference in the thermodynamic stability of the two isomers and the different reactivity is only due to a different activation enthalpy, arising by a different mechanism. Therefore, **Mt** reacts via the methyl migration mechanism; the low reactivity is due to the effect of the trans σ donor ligand (I^-) by decreasing the migration aptitude of the methyl as reported by Kubota et al. [31] and as expected on the basis of the calculations of activation energies performed by Berke and Hoffmann [32]. The ionic mechanism in complex **Mt** is not easy due to the different position of I^- in the intermediate ion pair (**In**). In fact, if I^- remains localized in the original position, it is far from CH_3 and cannot promote the insertion process.

5. Supplementary material

Complete listings of bond lengths and angles, anisotropic parameters, hydrogen atomic coordinates, observed and calculated structure factors for complexes **Mc** and **Mt** (20 pages) may be obtained from the authors upon request.

Acknowledgements

This work was supported by grants from the Consiglio Nazionale delle Ricerche (CNR, Rome, Italy) and the Ministero dell'Università e della Ricerca Scientifica e Tecnologica (MURST, Rome, Italy). We thank Professor V.G. Albano for helpful discussions.

References

[1] G. Cardaci, G. Reichenbach and G. Bellachioma, *Inorg. Chem., 23* (1984) 2936.
[2] G. Reichenbach and G. Bellachioma, *J. Chem. Soc. Dalton Trans.*, (1987) 519.
[3] G. Cardaci, G. Reichenbach, G. Bellachioma, B. Wassink, and M.C. Baird, *Organometallics, 7* (1988) 2475.
[4] G. Bellachioma, G. Cardaci, C. Jablonski, A. Macchioni and G. Reichenbach, *Inorg. Chem., 32* (1993) 2404.
[5] M. Pankowski and M. Bigorgne, *J. Organomet. Chem., 251* (1983) 333.
[6] S.C. Wright and M.C. Baird, *J. Am. Chem. Soc., 107* (1985) 6899.
[7] G. Reichenbach, G. Cardaci and G. Bellachioma, *J. Chem. Soc. Dalton Trans.*, (1982) 847.
[8] F. Calderazzo, *Angew. Chem. Int. Ed. Engl., 16* (1977) 299 and reference cited therein.
[9] J.J. Alexander, in F.R. Hartley and S. Patai (eds.), *The Chemistry of the Metal–Metal Bond*, Vol. 2, Wiley, New York, 1985, pp. 339–400.
[10] M. Pankowski and M. Bigorgne, *J. Organomet. Chem., 30* (1971) 227.

[11] M. Pankowski and M. Bigorgne, *VIII ICOMT*, Kyoto, Japan, 1977.
[12] G. Bellachioma, G. Cardaci, A. Macchioni and G. Reichenbach, *Inorg. Chem., 31* (1992) 3018.
[13] A. Weissberger and E.S. Proskauer, *Techniques of Organic Chemistry: Organic Solvents*, Vol. VII, Interscience, New York, 2nd edn., 1955.
[14] G. Reichenbach, G. Innorta and A. Foffani, *Inorg. Chim. Acta, 3* (1969) 139. G. Reichenbach, *J. Organomet. Chem., 31* (1971) 103.
[15] (a) E. Wilhelm and R. Battino, *J. Chem. Thermodyn., 5* (1973) 117. (b) F. Calderazzo and F.A. Cotton, *Inorg. Chem., 1* (1962) 30.
[16] R.C. Weats, *Handbook of Chemistry and Physics*, CRC Press, Boca Raton, FL, 67th edn., 1986–87, p. D214.
[17] G.M. Sheldrick, SHELXS86, *Acta Crystallogr. Sect. A:, 46* (1990) 467.
[18] G.M. Sheldrick, SHELXL93, *Program for Crystal Structure Refinement*, University of Göttingen, Germany, 1993.
[19] G. Bellachioma, G. Cardaci, A. Macchioni and P.F. Zanazzi, *Inorg. Chem., 32* (1993) 547.
[20] G. Bellachioma, G. Cardaci and P.F. Zanazzi, *Organometallics, 7* (1988) 172.
[21] A.G. Orpen, L. Brammer, F.H. Allen, O. Kennard, D.G. Watson and R. Taylor, *J. Chem. Soc. Dalton Trans.*, (1989) S1.
[22] Cambridge Structural Database.
[23] D. Ginderow, *Acta Crystallogr. Sect. B:, 36* (1980) 1950.
[24] H. Berke, R. Birk, G. Huttner and L. Zsolnai, *Z. Naturforsch. Teil B:, 39* (1984) 1380.
[25] A.A. Frost and R.G. Pearson, *Kinetics and Mechanism*, Wiley, New York, 2nd edn., 1961, pp. 142–147.
[26] G. Bellachioma, G. Cardaci, A. Macchioni and G. Reichenbach, *J. Organomet. Chem., 427* (1992) C37.
[27] G. Bellachioma, G. Cardaci, A. Macchioni and G. Reichenbach, *Gazz. Chim. Ital., 121* (1991) 101. G. Bellachioma, G. Cardaci, A. Macchioni and G. Reichenbach, *Inorg. Chem., 31* (1992) 63.
[28] D. McDaniels and C.R. Smoot, *J. Phys. Chem., 60* (1956) 966.
[29] A. Wojcicki, *Advanced Organometallic Chemistry*, Academic Press, New York, 1973, pp. 87–145. R.W. Glyde and R.J. Mawhy, *Inorg. Chem., 10* (1971) 854. R.J. Mawhy, F. Basolo and R.G. Pearson, *J. Am. Chem. Soc., 86* (1964) 3994. I.S. Butler, F. Basolo and R.G. Pearson, *Inorg. Chem., 6* (1967) 2074.
[30] G. Reichenbach, personal communication, 1996.
[31] M. Kubota, T.M. McClesky, R.K. Hayashi and C.G. Webb, *J. Am. Chem. Soc., 109* (1987) 7569.
[32] H. Berke and R. Hoffmann, *J. Am. Chem. Soc., 100* (1978) 7224.